Chemistry & Biology, Vol. 11, 1431–1443, October, 2004, ©2004 Elsevier Ltd. All rights reserved. DOI 10.1016/j.chembiol.2004.08.013

Wide-Angle X-Ray Solution Scattering as a Probe of Ligand-Induced Conformational Changes in Proteins

R.F. Fischetti,[1,2] D.J. Rodi,[1] D.B. Gore,[3] and L. Makowski[1,*]
[1]Biosciences Division
[2]GM/CA-CAT, Advanced Photon Source
Biosciences Division
[3]Bio-CAT, Advanced Photon Source
Argonne National Laboratory
9700 South Cass Avenue
Argonne, Illinois 60439

Summary

A chemical genetics approach to functional analysis of gene products utilizes high-throughput target-based screens of compound libraries to identify ligands that modulate the activity of proteins of interest. Candidates are further screened using functional assays designed specifically for the protein—and function—of interest, suffering from the need to customize the assay to each protein. An alternative strategy is to utilize a probe to detect the structural changes that usually accompany binding of a functional ligand. Wide-angle X-ray scattering from proteins provides a means to identify a broad range of ligand-induced changes in secondary, tertiary, and quaternary structure. The speed and accuracy of data acquisition, combined with the label-free targets and binding conditions achievable, indicate that WAXS is well suited as a moderate-throughput assay in the detection and analysis of protein-ligand interactions.

Introduction

Chemical genetics is the study of protein function using exogenous ligands to alter protein function, enabling the analysis of the biological consequences of the resulting changes [2]. A prerequisite for this approach is the identification of ligands that modulate the function of each protein of interest. Target-based screens based on binding affinity are used to identify ligands from compound libraries of up to 1 million compounds, typically yielding 10–100 candidate ligands [3]. The subsequent functionality tests of these candidate ligands represent a potential bottleneck in the development of chemical genetics. In vivo screens can detect phenotypic changes resulting from ligand action but may provide ambiguous results if the ligand tested binds to other gene products, or false negatives if parallel pathways are active under the conditions of the assay. In vitro screens may require use of a custom assay designed for a specific function, and assays for many relevant functions do not yet exist. An alternative approach is the use of a generic biophysical method that can detect the structural changes in a protein that usually accompany the binding of a functional ligand. Unfortunately, most approaches are sensitive to limited classes of structural change. For instance, circular dichroism is insensitive to changes that do not alter protein secondary structure [4], and small angle X-ray scattering (SAXS) cannot detect changes that do not alter the radius of gyration.

Wide-angle X-ray scattering (WAXS) from proteins in solution has been shown to generate data that are sensitive to secondary, tertiary, and quaternary structural elements [1]. X-ray scattering data from proteins in solution correspond roughly to the spherical average of data collected by X-ray crystallography. Scattering at small angles (SAXS) reflects the overall size and shape of the protein. SAXS from proteins in solution [5] has been used to determine the radius of gyration of proteins and protein complexes, and has proven effective at identifying small changes in radius of gyration due to ligand binding [e.g., 6–8]. Scattering at progressively larger (wider) angles corresponds to progressively more detailed structural features in the protein. The information present in the SAXS data generally reflects global size and shape, but conformational changes that do not lead to changes in radius of gyration are difficult to detect. WAXS is an extension of SAXS in which data are collected to higher scattering angles. Although WAXS data are significantly weaker than SAXS data, they can be collected using less than 200 μl of solution volume with protein concentrations of 5–10 mg/ml in less than 30 s with the high flux available at a third generation synchrotron X-ray source [1, 9]. Higher concentrations generally result in data with higher signal to noise ratio. Changes in WAXS data reflect changes in quarternary, tertiary or secondary structure, providing them with the potential for being a sensitive, global method for detecting ligand-induced structural changes in proteins.

To evaluate the potential of WAXS as a moderate-throughput screen of ligand-induced structural changes, the WAXS patterns from four proteins that undergo structural changes on binding a functional ligand were measured and analyzed. The observed differences indicated significant structural changes were occurring in the proteins in response to ligand binding. Comparison of these differences with differences calculated from crystallographic coordinates demonstrated that the scattering changes detected in the WAXS data are consistent with that predicted from the crystal structures of the proteins in the presence and absence of ligand.

For WAXS to be an effective tool for chemical genetics it must be able to distinguish a functional interaction from a nonfunctional interaction. WAXS is a sensitive tool for detection of the structural changes in proteins that accompany functional changes, thereby providing an indirect assay for functional interactions with small molecules. Some change in WAXS data could occur upon ligand binding even in the absence of structural change in the protein, but the magnitude of that change increases substantially when structural changes are induced by that binding. WAXS intensity differences calculated from crystallographic coordinates of apo and ligand-bound forms of proteins are shown here to corre-

*Correspondence: imakowski@anl.gov

spond well with measured differences. To estimate the intensity difference that would occur upon ligand binding in the absence of a structural change (i.e., differences emanating from the now protein-bound ligand), crystallographic coordinates of the ligand-bound form of the protein plus and minus the ligand were used to calculate solution scattering. As will be shown, the predicted intensity changes are much greater when a ligand induces a structural change than when it does not. Only for ligands with a molecular weight comprising greater than 2% of the total protein-ligand molecular weight (around 700 Da for a target protein of 35 KDa) does this distinction start to become difficult to make on the basis of WAXS data alone. However, even for that scenario, ligands that induce structural change will induce greater change in intensity than those that do not, providing a means to identify functionally active ligands.

Crystallographic coordinates are not required for the analysis of WAXS data. The magnitude of structural change can be estimated directly from the WAXS data. The precise form of that change at atomic resolution cannot be inferred, although changes in α-helix and β sheet content can be estimated (R.F.F., unpublished data). Furthermore, WAXS patterns generated computationally from crystal coordinates [10] predict that an even wider range of protein function altering interactions are amenable to detection via WAXS analysis. This method can be applied to almost any protein in solution with no need for chemical modification to facilitate either protein or small molecule ligand detection. These proof-of-concept data demonstrate that wide-angle X-ray scattering (WAXS) from proteins in solution can be implemented as a sensitive, moderate-throughput probe of ligand-induced structural changes for the identification of functional ligands.

Results and Discussion

Pairs of structures corresponding to proteins plus and minus ligand were selected from the Protein Data Bank (http://www.rcsb.org/pdb/) on the basis of the observed range of movement of the protein on ligand binding as calculated from the crystallographic coordinates using the web server DALI [11], paying particular attention to choosing proteins that undergo different ranges of movement, ranging from large domain shifts to secondary structure rearrangements to relatively small chain movements.

Ligand-Induced Domain Rotation: Transferrin

Crystal structure determination of several transferrins—plasma iron transport proteins—has revealed them to be made up of two lobes of very similar structure, each containing a high-affinity iron binding site and representing the N- and C-terminal halves of the molecule. The structure of the apo and ligand-bound forms of the N-terminal half of human transferrin have been determined by X-ray crystallography. The N-terminal half undergoes a 63° rotation of the N2 domain (residues 1–93 and 247–315) relative to the N1 domain (residues 94–246) in response to binding of ferric ions [12]. Comparison of the structures of these two forms is shown in Figure 1A. Conversion from the "open" apo form on the left to the "closed" ligand-bound form on the right occurs by bending around a hinge between the two domains in a "Venus flytrap"-like motion [13]. The protein conformation within each of the domains remains essentially unchanged on ligand binding with the exception of a shift in a mobile loop in the N2 domain and some alterations of the side chain conformations in the binding cleft [12].

WAXS data were collected from a solution of apobovine transferrin and from an identical sample in which the iron binding site was saturated [14]. Scattering patterns were collected and background from capillary and solvent were removed as described previously [1]. Figure 1B contains the observed WAXS scattering data from the two solutions, apo and ligand-bound transferrin. Figure 1C contains the calculated difference curve (black curve) between the two measured scattering curves in Figure 1B. After generation of a matched pair of scattering curves (apo and ligand-bound) for transferrin using CRYSOL and the crystallographic coordinates, a difference curve was calculated from this in silico pair of curves (red curve in Figure 1C) and compared to that calculated from the actual observed scattering patterns. The degree of intensity change that would occur on binding of ligand in the absence of an induced structural change was estimated by calculating the solution scattering from the ligand-bound form plus and minus the ligand. This difference is shown as a broken red line in Figure 1C. The relatively small size of this change demonstrates that protein structural change is responsible for virtually all of the observed change in intensity upon ligand binding.

X-ray scattering from solutions of proteins corresponds roughly to the spherical average of data collected from a crystal, thus containing significantly less information than a comparable crystallographic data set. Nevertheless, it provides information about the structure at multiple length scales, including the scale of the entire molecule, tertiary structures, and secondary structures. These patterns are circularly symmetric when collected with a two-dimensional detector after polarization correction. The one-dimensional plots in the Figures 1B and 1C correspond to a corrected circular average of the observed intensity. The left-hand edge of these plots corresponds to the center of the diffraction pattern, with progressively wider angle data plotted out along the abscissa. The circularly averaged WAXS data are plotted as a function of (1/d) with units of $Å^{-1}$. This corresponds to the reciprocal relationship between the scale of a structural feature in the protein and the distance from the center of the diffraction pattern to the peak of intensity arising from this feature. For instance, intensity occurring at $1/d = 0.1$ $Å^{-1}$ arises from features having a length scale of about 10 Å. Since α helices pack about 10 Å center-to-center, α-helical proteins usually exhibit relatively strong scattering at a spacing of $1/d = 0.1$ $Å^{-1}$. Small angle scattering (SAXS) data ($1/d \leq 0.01$ $Å^{-1}$) provide information about the size and shape of a protein molecule. In particular, the radius of gyration of a protein (defined as the average distance to the center of mass) can be obtained from this kind of data. At higher scattering angles, the features observed in the scattering patterns correspond to features at progres-

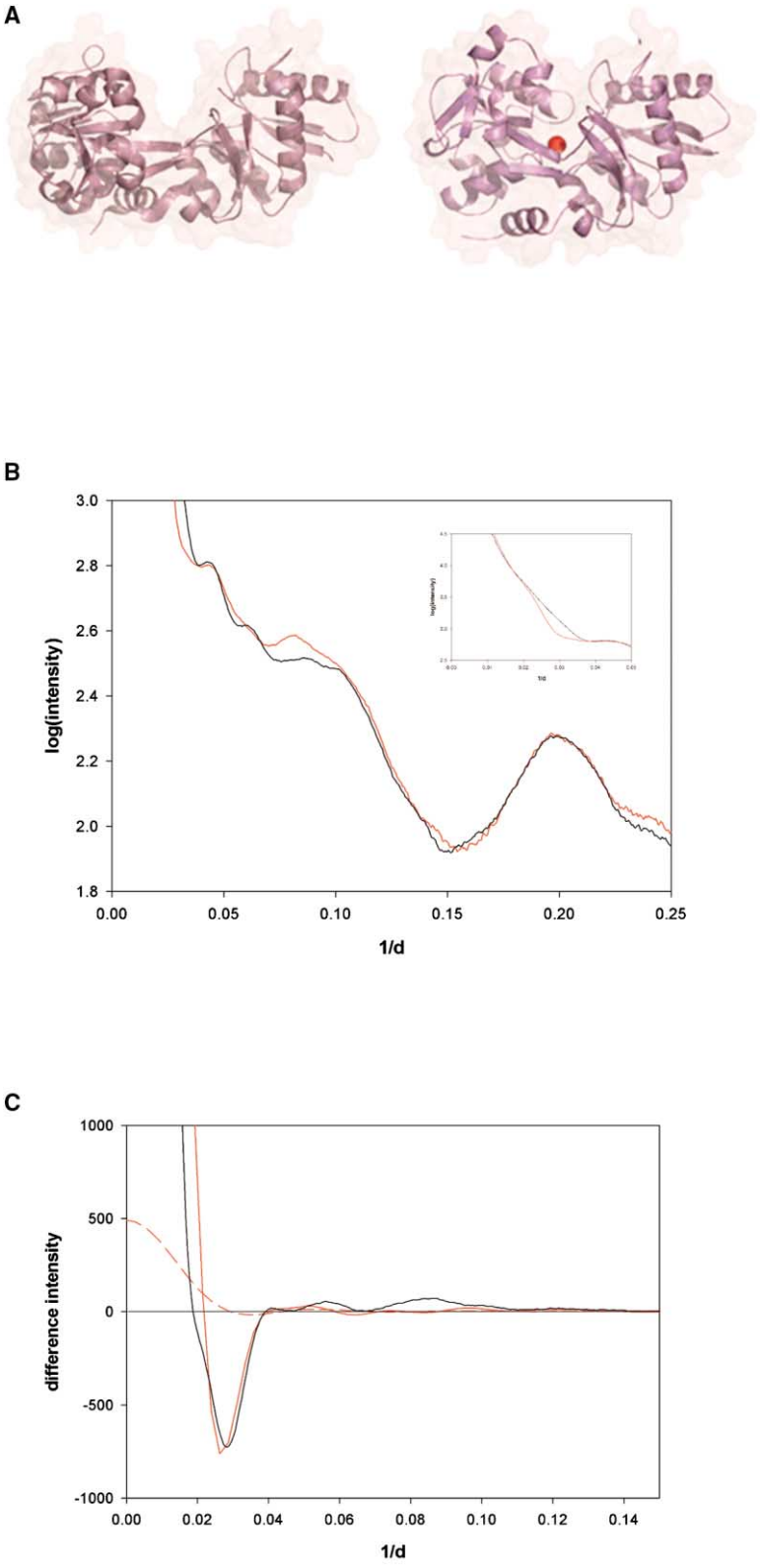

Figure 1. WAXS from Transferrin

(A) Computer renderings of the structure of the N-terminal lobe of transferrin as derived from crystallographic analyses of the protein in the presence (right) and absence (left) of iron. (Protein Data Bank [PDB] numbers 1BTJ and 1A8E.)

(B) Observed X-ray scattering intensity from transferrin before (black) and after (red) addition of ferric ammonium citrate. The region from 1/d of 0.01–0.05 is shown in the upper right corner inset at a smaller scale.

(C) Comparison of the observed (black) differences (ligand bound form minus apo form) between the X-ray intensity observed in the presence and absence of ligand, with that predicted from crystallographic coordinates (red) and that predicted to occur if the ligand-bound and apo forms were identical in structure except for the removal of ligand (red broken line).

sively finer levels of detail. Intensity differences observed in the 0.02–0.1 $Å^{-1}$ range correspond to movements of features separated by lengths of 50–10 Å.

Figure 2 contains the calculated difference intensities from Figure 1C (black) with error bars indicating the standard deviation as calculated from seven patterns collected from apotransferrin; seven from iron-saturated transferrin, and four each from the two corresponding

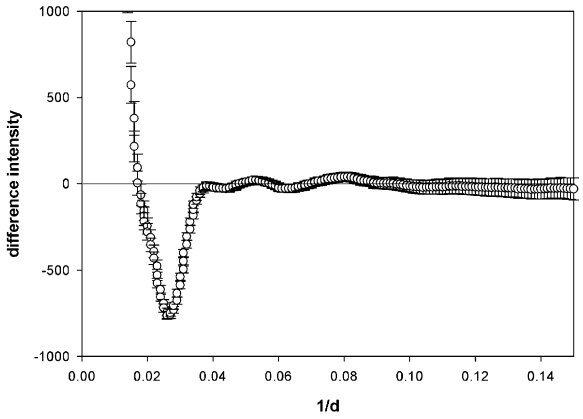

Figure 2. Uncertainty in Intensity Differences Derived from WAXS Data

Transferrin ligand bound form minus apo form, with error bars representing standard deviation as calculated from seven solution scattering patterns and four background patterns. The errors increase to the right in this figure because of the increased background due to solvent background scattering at those scattering angles. Error bars for all patterns reported here were similar in magnitude. In order to allow comparison of calculated and observed patterns, the error bars are not shown in later figures.

solvent solutions. The error bars are comparable to the random fluctuations apparent in the curves plotted in Figure 1, demonstrating that these fluctuations provide a reasonable measure of the errors in the data. Comparable error estimates have been made for the other differences intensities reported below. In order to allow ready comparisons between calculated and observed differences, these error estimates are not displayed.

The close correspondence between the calculated and observed difference intensities in Figure 1C indicates that the ligand-induced conformational changes accompanying the domain rotation in transferrin in solution are close to those observed in the differences in structure between the crystals of apo and ligand bound forms. Quantitative comparison between the calculated and observed differences do not provide meaningful numbers, as relatively small shifts in the positions of maxima and minima give rise to correspondingly low, discrepant correlation coefficients. The qualitative correspondence of features in the two difference plots indicate that the differences in solution are of similar nature and magnitude to those observed in crystals. The region of greatest change in intensity for this particular protein-ligand interaction is for spacings less than about 0.04 $Å^{-1}$. This corresponds to movements of large structures (a width of 1/0.04 = 25 Å) relative to one another, i.e., whole domains. A comparison of the crystallographic structures indicates that ligand binding is inducing large domain movements but relatively little secondary structure change, consistent with the location of the intensity differences. Higher-angle intensities change relatively little, as would be expected for a structural change that occurs with little or no rearrangement of individual side chains or secondary structure elements.

A quantitative measure of the conformational change due to ligand binding can be obtained using the DALI server [11]. Comparison of the C_α backbone of the apo and ligand-bound forms of transferrin using DALI shows an r.m.s. deviation of 5.7 Å. This large value is a reflection of the considerable structural change seen in the renderings of the two forms in Figure 1A and are clearly reflected in the WAXS data depicted in Figures 1B and 1C.

Hinge-Bending Motion: Maltose Binding Protein

An incrementally smaller structural change occurs in the maltose binding protein (MBP) in response to ligand binding. MBP is a part of the maltodextrin system of *E. coli* bacteria, which is responsible for the uptake and catabolism of maltodextrins. Like all periplasmic binding proteins, MBP is monomeric with two globular domains separated by a deep cleft. Each domain has a central β-pleated sheet, flanked on both sides by three parallel α helices. The maltodextrin ligand binding site is located at the base of this cleft between the two domains (Figure 3A). When bound to the protein with micromolar affinity, the sugar is buried deep within the cleft, almost completely inaccessible to the solvent. The conformational change between the bound and apo forms of MBP involves a 35° hinge bending movement accompanied by an 8° anticlockwise rotational twisting of the smaller N domain relative to the C domain (Figure 3A), similar to the flytrap movement of transferrin discussed above but smaller in magnitude. This rotation is accompanied by almost no conformational change within either domain—only a reorientation of the aromatic residues lining the binding cleft [15]. Comparison of the C_α backbone of the two forms of MBP using DALI shows an r.m.s. deviation of 1.7 Å. SAXS data collected to study the conformational change of MBP in solution [16] have confirmed that MBP is a monomer. The SAXS data collected were consistent with the possibility that MBP in solution undergoes conformational changes comparable to that observed by a comparison of the crystal structures.

The WAXS patterns collected in this study confirm those observations. WAXS patterns obtained from solutions of apo and ligand-bound maltose binding protein are shown in Figure 3B, with the ligand-induced difference patterns between the calculated scattering curves and the measured scattering data depicted in Figure 3C. Although the measured scattering from the two solutions is quite similar—reflecting the similarity of protein conformation in the two states—the difference is statistically significant (see Experimental Procedures). Comparison of the observed ligand-induced differences with those predicted on the basis of the two crystalline structures (Figure 3C) indicates good correspondence, supporting the statistical significance of the observed differences. The absolute values of the differences are significantly less than for transferrin, as would be expected from the smaller structural changes seen in a comparison of the crystalline form sets (apo and ligand-bound) of the two proteins (Figures 1A and 3A) and in the measures of structural similarity calculated with DALI. The largest intensity difference observed in the solution scattering is at somewhat smaller scattering angle than predicted from the crystallographic studies, suggesting that the rotation of domains in solution is somewhat larger in magnitude than predicted from a comparison of the respective crystal structures. Binding of glucose to MBP in the absence of a structural change

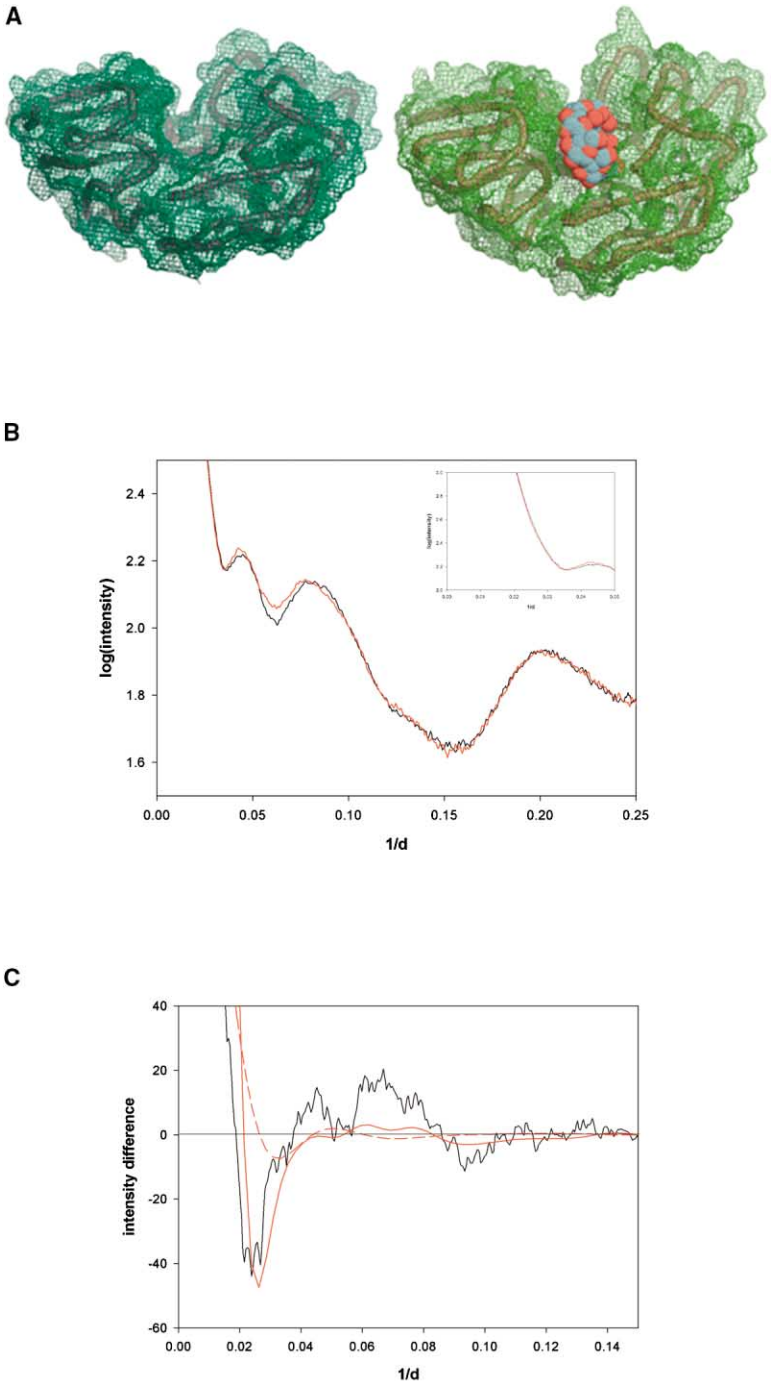

Figure 3. WAXS from Maltose Binding Protein

(A) Computer renderings of the structure of maltose binding protein (MBP) as derived from crystallographic analyses of the protein in the presence (right) and absence (left) of maltose. (PDB: 1OMP and 1DMB.)

(B) Observed X-ray scattering intensity from MBP before (black) and after (red) addition of ligand. The region from 1/d of 0.01–0.05 is shown in the upper right corner inset at a smaller scale.

(C) Comparison of the observed (black) differences (ligand bound form minus apo form) between the X-ray intensity observed in the presence and absence of ligand, with that predicted from crystallographic coordinates (red) and that predicted to occur if the ligand-bound and apo forms were identical in structure except for the removal of ligand (red broken line).

would give rise to barely observable intensity changes (red broken line in Figure 3C).

Change of the Shape of the Binding Cleft: Alcohol Dehydrogenase

Alcohol dehydrogenase (ADH), which oxidizes alcohols into aldehydes or ketones, requires the coenzyme NAD^+ as a hydrogen acceptor. The enzyme is a homodimer possessing two domains—an NAD^+ binding domain and a catalytic domain. The interdomain interface forms a cleft that contains the active, Zn^{2+}-containing catalytic site. When the NAD^+ binds the apo-enzyme there is a rotational change of about 7.5° around a hinge axis passing through the contact point of the α helices connecting the two domains (see Figure 4B). This change, classified as a shear motion according to Chothia and Lesk's classification of domain motions [17], results in a change in the shape of the cleft to accommodate the substrate. Analysis using DALI shows an overall r.m.s. deviation of 0.8 Å in the C_α atoms within the NAD^+ binding monomer of the enzyme.

As the NAD^+ coenzyme is the only element essential for inducing the conformational change of the enzyme from the open to the closed form, this makes the alcohol

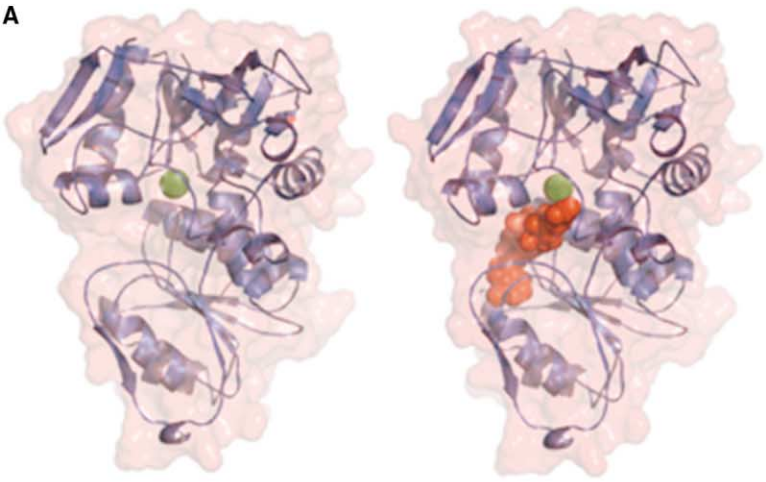

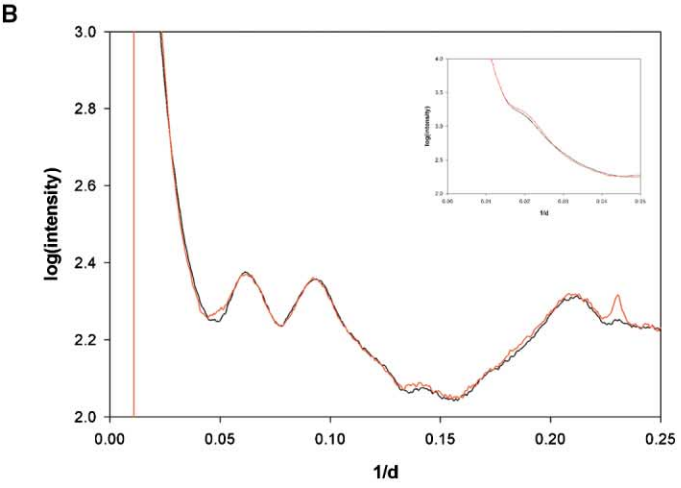

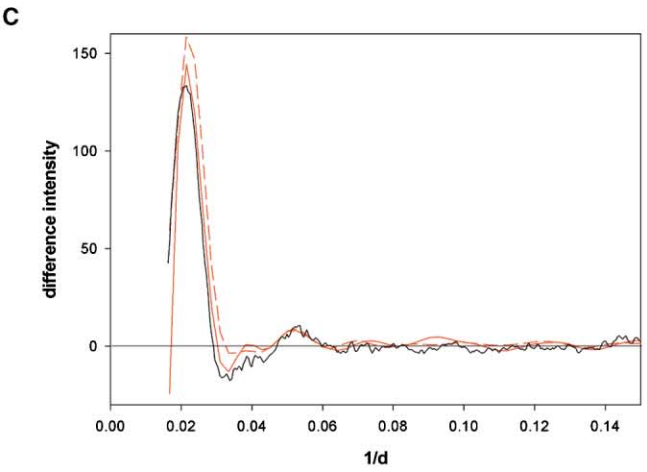

Figure 4. WAXS from Alcohol Dehydrogenase

(A) Computer renderings of the structure of alcohol dehydrogenase (ADH) as derived from crystallographic analyses of the protein in the presence (right) and absence (left) of NAD^+. (PDB: 1PED and 1KEV.)

(B) Observed X-ray scattering intensity from ADH before (black) and after (red) addition of ligand. The region from 1/d of 0.01–0.05 is shown in the upper right corner inset at a smaller scale.

(C) Comparison of the observed (black) differences (ligand bound form minus apo form) between the X-ray intensity observed in the presence and absence of ligand, with that predicted from crystallographic coordinates (red) and that predicted to occur if the ligand-bound and apo forms were identical in structure except for the removal of ligand (red broken line).

substrate irrelevant in the context of a conformational shift analysis. Figure 4B contains plots of the measured WAXS data from apo and NAD^+ bound yeast ADH. Figure 4C contains the difference plot between these two curves as compared to the difference plot obtained from the pair of scattering curves predicted from the crystallographic data using CRYSOL. Again, the form of the observed ligand-induced differences is close to that predicted from a comparison of the crystallographic structures. These data indicate that the protein undergoes a structural change in solution that is comparable to that observed between the two crystal forms. Because of its size (approximately 700 Da), the intensity change that would occur on binding of NAD^+ in the absence of a structural change would be comparable in magnitude to that observed (red broken line in Figure 4C).

Ligand-Induced Refolding: Calmodulin

Calmodulin is the primary eukaryotic intracellular calcium receptor and serves as a second messenger to regulate cellular responses to transient calcium fluxes. When activated by calcium binding, calmodulin is rendered capable of binding and activating a large number of intracellular proteins, components of multiple signal transduction pathways that regulate various processes such as muscle contraction and cytoskeletal activity. The calmodulin protein contains two calcium binding domains separated by a long central α-helix (Figure 5A, left side). Each domain consists of a pair of "EF-hand" calcium binding motifs. At resting cell calcium concentrations (typically 50–100 nM), these binding sites are largely unoccupied, but at the higher calcium concentrations that can be transiently induced by external stimuli, they bind calcium, inducing a large conformational change [18]. Binding of the four calcium ions to calmodulin is cooperative in nature [19, 20] and initiates the opening of a hydrophobic cleft within the four-helix bundle of each EF-hand, resulting in significant non-polar surface area exposure and the modulation of both the interaction between the two domains and the interactions between the protein and numerous regulatory partners within the cell. Calcium binding induces an increase in the level of ordered secondary structure as shown by a 12% increase in ellipticity at 222 nm measured by CD spectroscopy and a decrease in the Stokes radius of the protein of approximately 1.29 Å [19]. The r.m.s. deviation between the apo and ligand-bound forms of calmodulin is 5.6 Å as calculated by DALI, indicating a relatively large structural transition upon binding calcium. The crystal structure-predicted changes induced by binding are illustrated in Figure 5A.

The WAXS scattering curves measured from bovine brain calmodulin in the presence and absence of calcium are shown in Figure 5B. The observed intensities vary more slowly as a function of scattering angle because of the relatively small size of the protein. The most obvious change in scattering is at small angles where the central maximum is wider in scattering from the apo form (black) than the Ca^{2+}-bound form (red). This is indicative of an increase in the radius of gyration of the protein on binding to Ca^{2+} as predicted from the crystallographic structures. The scattering pattern differences induced by ligand binding as measured using WAXS (Figure 5C, black curve) are comparable to those predicted from the crystal structures using CRYSOL-generated scattering curves (Figure 5C, red curve).

Ligand-Induced WAXS Changes in Other Systems

The protein data bank now contains several examples of structure pairs consisting of proteins in the presence and absence of ligands. These crystal structure pairs can be used to predict the expected changes in WAXS patterns upon ligand binding using CRYSOL. Since the magnitudes of difference intensities resulting from ligand-induced structural changes in transferrin, maltose binding protein, alcohol dehydrogenase and calmodulin were predicted reasonably well using CRYSOL, we expect the intensity changes predicted from CRYSOL for other systems to similarly be a good reflection of the observations that would emerge from experimental studies of these systems as well. Consequently, CRYSOL can be used as a means of surveying a wider range of molecular systems to assess the potential power of WAXS for detecting functionally relevant structural changes.

Side Chain Reorientations: Adipocyte Lipid Binding Protein and Ricin

Adipocyte Lipid Binding Protein (ALBP) is expressed exclusively in adipose cells for the purpose of facilitating the uptake and utilization of hydrophobic lipids such as long chain fatty acids and retinoic acid [21]. The crystal structure of ALBP reveals the tertiary structure as that of a 'β-clam', consisting of two nearly orthogonal β sheets formed by ten antiparallel β strands, with a single helix-turn-helix motif between the A and B strands [22] (Figure 6A, left). These paired β sheets have a right-handed twist and surround an internal ligand binding site, similar to a number of extracellular and intracellular hydrophobic ligand binding proteins. ALBP binds the polyunsaturated fatty acid arachidonic acid (ACD) with high affinity ($K_D = 4.4\ \mu M$) [23]. The crystal structure of the ALBP-ACD complex demonstrates that the bound fatty acid lies completely within the cavity of ALBP [23]. A comparison of the apo versus ligand-bound forms of the protein (Figure 6A) demonstrates that small changes in protein conformation occur upon ligand binding, involving only reorientation of a few side chains (specifically R106, R126 and Y128). The r.m.s. deviation between the two forms is 0.5 Å [11]. This places the ALBP conformation shift in a different category from the measured proteins above, as there is almost no discernable change in position for any of the Cα backbone atoms upon ligand binding. Nevertheless, as shown in Figure 6B, the changes in intensities predicted for this structural change using CRYSOL are sufficiently large to indicate that, based on the results reported above; they would be readily observable using WAXS.

Ricin is an unusually cytotoxic plant protein (a single molecule can kill one mammalian cell [24]) that attacks ribosomes by hydrolyzing a specific adenine base from a highly conserved, single-stranded 28S rRNA hairpin. This hydrolytic reaction disrupts the binding of ribosomes to elongation factors and inhibits protein synthe-

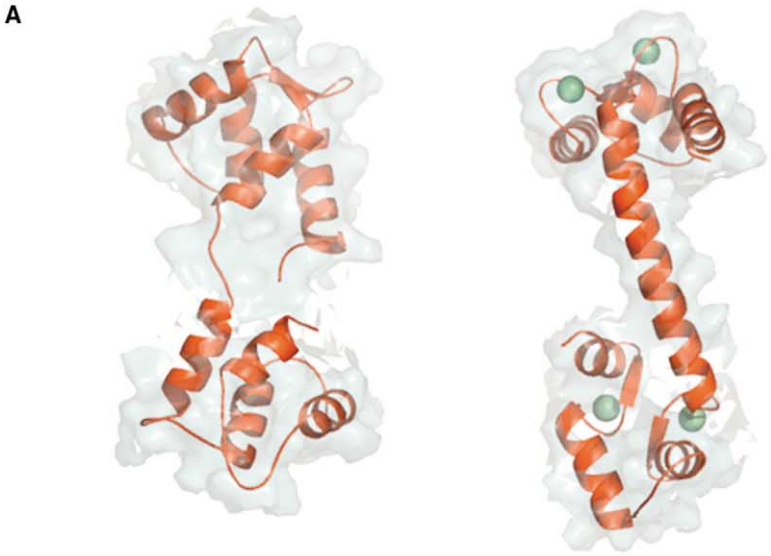

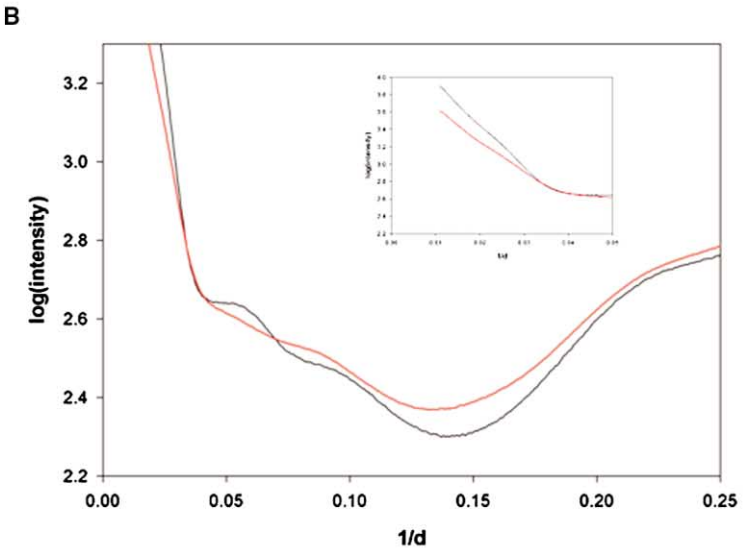

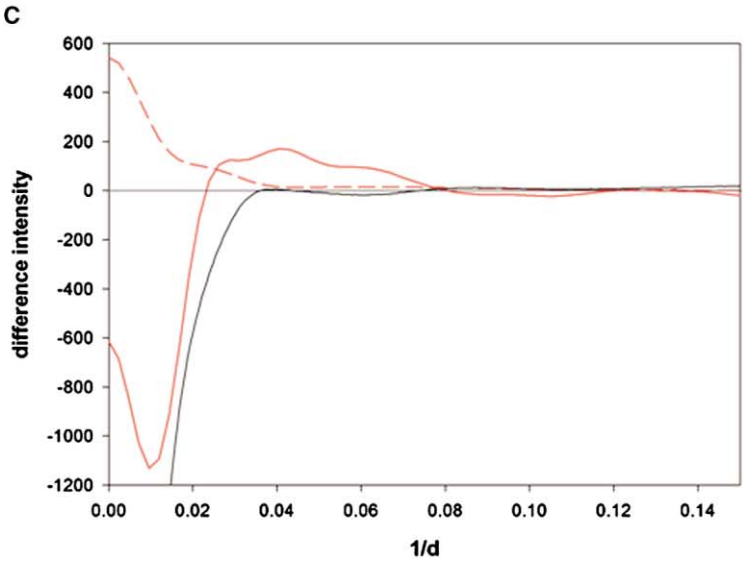

Figure 5. WAXS from Calmodulin

(A) Computer renderings of the structure of calmodulin as derived from crystallographic analyses of the protein in the presence (right) and absence (left) of Ca^{2+}. (PDB: 1CFD and 1CLL.)

(B) Observed X-ray scattering intensity from calmodulin before (red) and after (black) addition of EDTA. Color coding of this figure is such that the ligand bound form ($+Ca^{2+}$) protein is red, as in Figures 1–3. The region from 1/d of 0.01–0.05 is shown in the upper right corner inset at a smaller scale.

(C) Comparison of the observed (black) differences (ligand bound form minus apo form) between the X-ray intensity observed in the presence and absence of ligand, with that predicted from crystallographic coordinates (red) and that predicted to occur if the ligand-bound and apo forms were identical in structure except for the removal of ligand (red broken line).

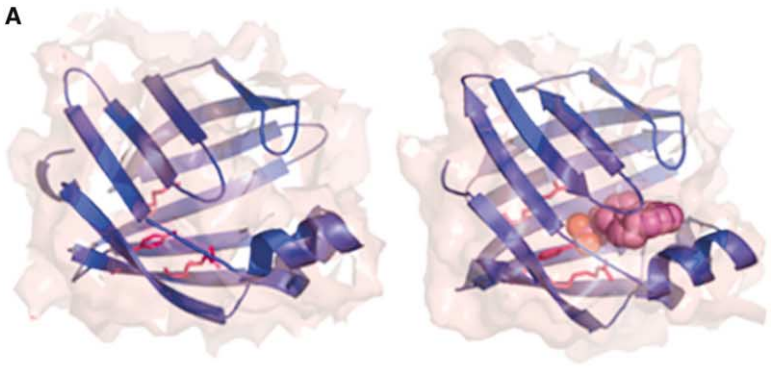

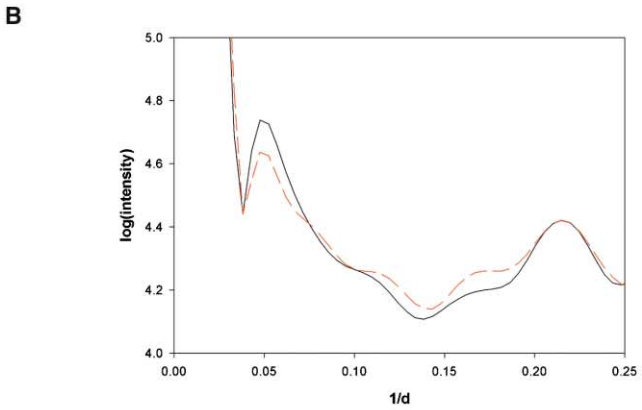

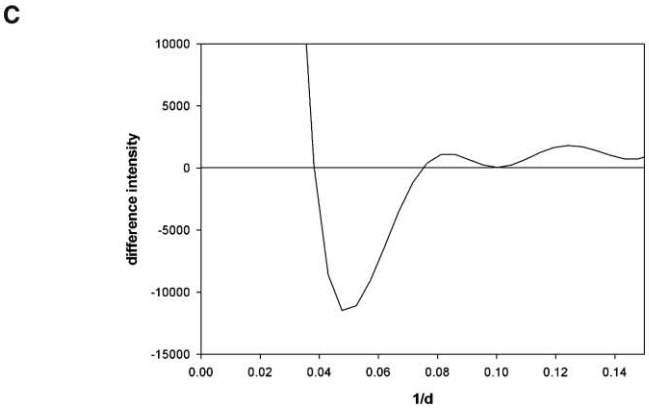

Figure 6. Predicted WAXS Pattern from Adipocyte Lipid Binding Protein

(A) Computer renderings of the structure of adipocyte lipid binding protein (ALBP) as derived from crystallographic analyses of the protein in the presence (right) and absence (left) of the ligand arachidonic acid. (PDB: 1ALB AND 1ADL.)

(B) Predicted X-ray scattering intensity from ALBP before (black) and after (red) addition of arachidonic acid.

(C) Comparison of the predicted differences (ligand bound form minus apo form) between the X-ray intensity observed in the presence and absence of ligand.

sis [25]. The protein is a heterodimer consisting of a catalytic 267-residue cytotoxic A chain linked by a disulfide bond to a lectin B chain of 262 residues, the latter of which is used by the protein to locate and bind to cell surfaces. The X-ray crystal structure of the catalytic ricin toxic A chain (RTA) had been reported by two groups to consist of three adjacent domains, each with a distinctive tertiary fold (see top of Figure 7A) [26, 27]. X-ray crystal structures of RTA complexed with AMP [28] and the ricin inhibitor neopterin, respectively, [29] have been obtained in an attempt to elucidate the nature of the binding site. Binding of AMP to the active site of an RTA point mutant results in a protein structure left essentially unchanged from that of the apoenzyme (Figure 7A, lower left). The bound purine makes few hydrogen bonds, and the phosphate moiety appears to form no direct interactions with the protein whatsoever [28]. The r.m.s. deviation between RTA and the RTA/AMP complex is 0.2 Å, the lowest value calculated for the protein set analyzed herein. The RTA/neopterin interaction (Figure 7A, lower right), although similar in its lack of impact upon backbone chain position, results in the displacement of the Y80 side chain, with a resulting r.m.s.d. of 0.6 Å by comparison. The predicted WAXS patterns plotted in Figure 7B for all three structures (apo RTA, AMP/RTA, and neopterin/RTA) indicate that these structural changes are adequate to result in observable changes in WAXS data.

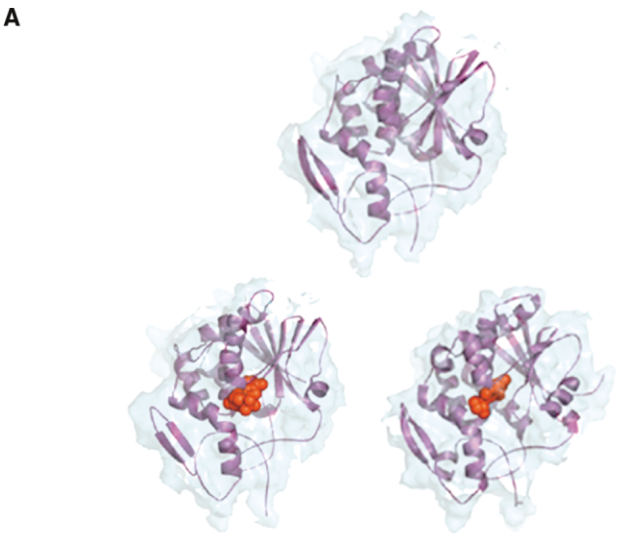

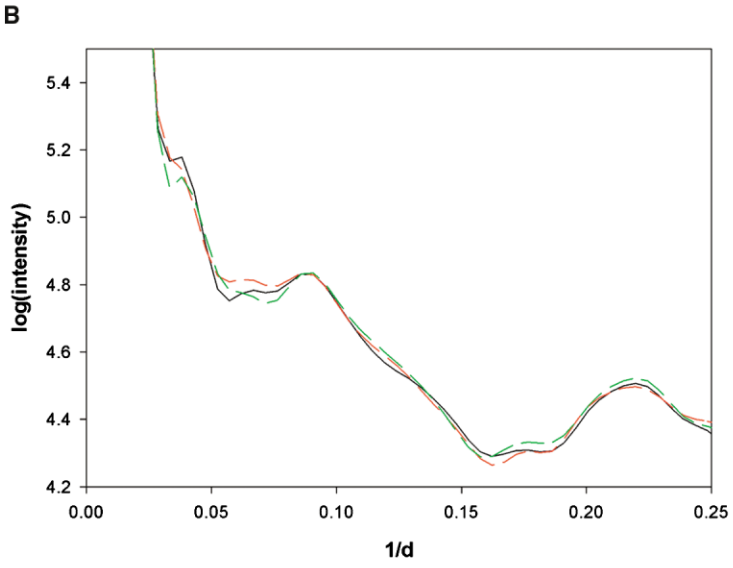

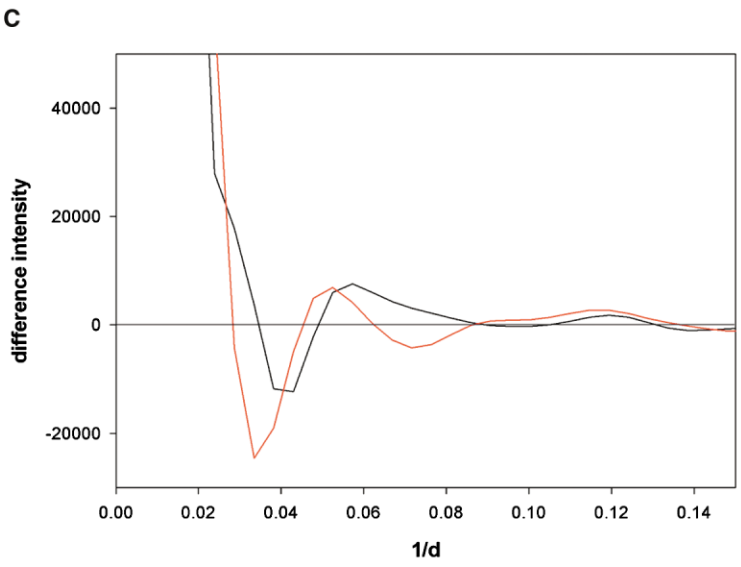

Figure 7. Predicted WAXS Pattern from Ricin

(A) Computer renderings of the structure of ricin as derived from crystallographic analyses of the apoprotein, in the presence of neopterin (lower right) and AMP (lower left). (PDB: 1OBS, 1OBT, and 1BRS.)

(B) Predicted X-ray scattering intensity from three crystal forms of ricin, the apo form (black curve), the AMP-bound form (red curve), and the neopterin bound form (green curve).

(C) Comparison of the predicted differences (ligand bound form minus apo form) between the X-ray intensity observed in the presence and absence of either AMP (black curve) or neopterin (red curve).

Detection of Functional Protein-Ligand Interactions

Functional interaction of a small molecule with a protein necessarily results in a change in the structure of the protein [17]. This change may be relatively large, involving domain rotations or domain refolding; or small and localized, involving the reorientation of only a few side chains. Structural changes that involve refolding can usually be observed using any of a variety of spectroscopic methods, most notably circular dichroism. Structural changes involving domain rotations or side chain shifts are more difficult to observe. Solution structures of proteins can be obtained using NMR, but require extensive data collection and analyses [30]. Small-angle scattering (SAXS) can readily observe structural changes that result in a change in the radius of gyration, but not all domain rotations will be detectable at these scattering angles and small side chain alterations will be undetectable.

A combination of SAXS and WAXS can provide a characterization of the form of structural change induced by ligand binding, even in the absence of information from crystallographic data. SAXS data yield an indication of change in radius of gyration; intensity changes at moderate spacings (0.01–0.05 $Å^{-1}$) provide information about domain shifts; and wider angle intensity (0.05–0.25 $Å^{-1}$) contributes information about changes in secondary structure. For instance, the intensity at a spacing of about 0.1 $Å^{-1}$ correlates with the proportion of α-helix in a protein (R.F.F., unpublished data). A complete analysis of the ligand-induced intensity change can consequently provide a measure of both the magnitude and form of the corresponding structural change. This method can be used to detect structural changes for interactions with dissociation constants in the millimolar range or below. For example, detection of 90% binding of a 20 KDa protein at 10 mg/mL by a ligand present in 10-fold molar excess can be achieved with WAXS, an interaction with a dissociation constant of roughly 5 mM. Given the broad range of protein concentrations compatible with this technique (5 mg/mL and above), the ability to work with excess ligand, and the power to detect interactions in the absence of immobilization of either binding partner, this approach furnishes significant advantages over presently utilized methodologies for the detection of functional interactions.

The range of ligand-induced changes in structure studied here consistently resulted in changes in solution scattering at scattering angles slightly smaller than those predicted from the corresponding crystallographic structures. This result is consistent with the idea that ligand-induced domain movements are somewhat larger than suggested by a comparison of the crystallographic structures of these proteins in the presence and absence of ligand. It has been previously pointed out that although X-ray crystallography can provide an accurate description of molecular structure as it exists in the crystal lattice, orientation of domains can be influenced by crystal packing forces. As a result, the position of domains as established by X-ray crystallography may differ from the average position that is observed in solution [31]. In this work, we have observed that the scale of structural changes observed in solution is consistently larger than that predicted from a comparison of crystal structures.

Here we have demonstrated that WAXS can detect ligand-induced structural changes that involve domain movements as well those that involve smaller changes such as side chain rearrangements. Collection of data needed to detect these structural changes takes approximately 30 s at a third generation synchrotron source and is compatible with a wide range of solution conditions for nonchemically modified protein-ligand pairs.

Significance

A major bottleneck in the use of chemical genetics is the detection of functional interactions of small molecules with proteins. Candidate compounds identified through binding assays are further screened using a functional assay designed specifically for the protein, and function, of interest. This approach suffers from the need to customize the assay to the protein of interest. As ligand binding may induce large structural changes in the receptor protein, such as the movement of loops or even large domains, or produce small-scale changes such as the reorientation of side chains while leaving the backbone structure relatively intact, an alternative strategy is to utilize an in vitro biophysical probe that can detect the structural changes that usually accompany the binding of a functional ligand. Wide angle X-ray scattering from proteins in solution provides the means to identify ligand-induced changes encompassing secondary, tertiary, or quaternary structure. Given the sensitivity of X-ray scattering to protein conformation and the fact that most proteins undergo some degree of conformational change, either local or global, on binding a functional ligand, WAXS has the potential to serve as a valuable new tool in the analysis of protein/small molecule interactions in solution under conditions that require no chemical or physical alteration of either binding partner. The speed and accuracy of data acquisition combined with the broad range of label-free targets and binding conditions achievable with this technique indicate that WAXS is well suited as a moderate-throughput assay in the detection and analysis of protein-ligand interactions.

Experimental Procedures

Protein Preparation

All proteins were treated with excess concentrations of ligand using conditions established within the literature as accomplishing saturation of their respective ligand binding sites. Bovine erythrocyte hemoglobin (Calobiochem) was dissolved in sterile PBS (phosphate-buffered saline; 137 mM NaCl, 2.7 mM KCl, 10 mM Na2HPO4, and 2 mM KH2PO4) from Biowhittaker to a final concentration of 48 mg/mL and centrifuged at 4°C through a Nanosep centrifugal device (molecular weight cutoff = 300 kDa; Pall Corporation) for 10 min prior to beam exposure to remove high-molecular weight protein aggregates from solution. Horse skeletal muscle myoglobin (Sigma-Aldrich) was dissolved in sterile deionized water to a final concentration of 20 mg/mL. Bovine apotransferrin (Serologicals Corp.) was dissolved in 25 mM Tris-HCl (pH 8.0) to 40 mg/mL. One-half of this solution was treated with a 0.4× volume of ferric ammonium citrate (40 mg/mL in 10 mM sodium bicarbonate) for 4 hr at room tempera-

ture to saturate the iron binding site on the transferring molecule [14]. Maltose binding protein (New England Biolabs) was put through a buffer exchange spin column and concentrated to a final 13.5 mg/mL in 50 mM Tris-HCl (pH 7.5) and 100 mM KCl. A 1 M stock solution of maltose (Sigma-Aldrich) in the same buffer was added to a final concentration of 1 mM to generate the ligand bound form. Alcohol dehydrogenase from bakers yeast (Sigma-Aldrich) was dissolved in 100 mM sodium citrate (pH 6.0), 1 mM zinc acetate, and 0.1 mM dithiothreitol, to a final concentration of 15 mg/mL. β-nicotinamide adenine dinucleotide (NAD^+; Sigma-Aldrich) from a stock solution in the same buffer was added to a final concentration of 1 mM to generate the ligand bound form. Crystalline calcium-bound bovine brain calmodulin (Calbiochem) was dissolved in sterile deionized water to a final concentration of 13.3 mg/mL in 20 mM HEPES (pH 7.0) and 30 μM calcium chloride. The apo form of the protein was generated by calcium chelation through the addition of EDTA to a final concentration of 25 mM.

X-Ray Scattering Data

Wide-angle X-ray scattering (WAXS) data were collected at the BioCAT undulator beam line (18ID) at the Advanced Photon Source (APS), Argonne, IL [32]. The experimental layout was arranged as previously described [1] except that the specimen chamber was enclosed in a Helium atmosphere to minimize air scatter. The sample cell consisted of a thin-walled quartz capillary (1 mm I.D.) attached to a programmable pump (Hamilton Microlab 500 series) that was adjusted to deliver continuous flow through the capillary during data collection. The ambient temperature of the air surrounding the capillary was kept lower than room temperature by attachment of a 5° bath to the brass capillary holder to minimize protein denaturation during data collection. The X-ray scattering pattern was recorded with a MAR165 2kx2k CCD detector. The specimen to detector distance was 147.5 mm. The X-ray beam was focused to 40 × 180 μm (Vertical × Horizontal, FWHM) at the detector. Due to the long depth of focus the beam was only slightly larger at the specimen. The beamline is capable of delivering approximately 2×10^{13} photons/sec/100 mA of beam current. As previous experience on the BioCAT beamline has demonstrated that proteins under a variety of physical conditions are damaged after exposure times of a few tenths of a second to a few seconds at these intensity levels, in these experiments 20–36 μm thin aluminum foils were used as X-ray beam attenuators to control the incident beam flux. The data were collected at protein concentrations ranging from 12.6–48 mg/mL (see figure legends and Experimental Procedures for specific values and buffer conditions). A minimum of four and seven independent 5 s exposures were taken of the background buffer and protein solutions, respectively, to reduce noise levels. Several measurements of empty capillary scatter were also taken for subtraction purposes. Exposures from sample and buffer were alternated to minimize the possible effects of drift in any experimental parameter.

Data Processing

The two-dimensional scattering patterns collected in tiff format from the CCD detector were integrated radially to one-dimensional scattering intensity profiles using the program Fit2D version 9.129 [33–35]. The origin of the diffraction pattern was determined by calculating the center of powder diffraction rings from lead stearate powder. Calculation of scatter from protein was performed as previously described [1] discarding outlier patterns due to the presence of small bubbles in the quartz capillary sample holder. Small ambiguities (less than one-tenth of one percent) in the relative scaling of the scattering from solvent, capillary, and protein solution lead to some uncertainty in the scaling of higher angle features relative to the features in the 0.1 A-1 range. These were resolved on the basis of self-consistency of features in patterns from homologous proteins.

Seven data sets were collected for each protein with and without ligand and used to calculate mean scattering intensity and standard deviations at each diffraction angle. The noise level apparent in the observed scattering distributions or difference intensities in the figures provides an accurate measure of these standard deviations: there is a high degree of correlation between the scattering intensity at adjacent points in these (highly oversampled) plots but the data collected at adjacent points are independent of one another. Consequently, the random fluctuations exhibited by the plots trace out the range of intensity consistent with the multiple data sets, thereby reflecting the magnitude of errors intrinsic to the data sets.

Prediction of Scatter Pattern from Protein Based on Crystallographic Coordinates

Predictions of WAXS from proteins can be generated from their atomic coordinates when their crystallographic structures are available using the program CRYSOL [10]. This calculation makes standard assumptions about the hydration shell and rigidity of the protein. Discrepancies between calculated and observed WAXS patterns may be interpretable on the basis of differences in protein structure between crystal and solution including differences in average positions of atoms in the structure and its flexibility [1]. WAXS patterns were calculated from crystallographic coordinates using the program CRYSOL [10] (version 2.3, http://www.emblhamburg.de/ExternalInfo/Research/Sax/manual_crysol.html) using 50 spherical harmonics and default parameters for calculation of solvation shell and particle envelope. A maximum allowed number of Fibonacci grid points of 18 was used for all calculations. No attempt was made to directly fit the CRYSOL-calculated pattern to the experimental data.

Acknowledgments

The authors would like to thank the staff and scientists of Sector 18 at the APS for technical help and use of the facilities, S. Mandava for help in figure preparation, and P. Laible and D. Minh for helpful discussions. All protein renderings were carried out using PyMol [36]. This project was supported in part by a grant from the U.S. Department of Energy, Office of Biological and Environmental Sciences to D.J.R. Use of the Advanced Photon Source was supported by the U.S. Department of Energy, Basic Energy Sciences, Office of Science, under contract No. W-31-109-ENG-38. BioCAT is a National Institutes of Health-supported Research Center RR-08630.

Received: February 26, 2004
Revised: August 9, 2004
Accepted: August 10, 2004
Published: October 15, 2004

References

1. Fischetti, R.F., Rodi, D.J., Mirza, A., Irving, T.C., Kondrashkina, E., and Makowski, L. (2003). High resolution wide angle X-ray scattering of protein solutions: effects of beam dose on protein integrity. J. Synch. Res. *10*, 398–404.
2. Screiber, S.L. (1998). Chemical genetics resulting from a passion for synthetic organic chemistry. Bioorg. Med. Chem. *6*, 1127–1152.
3. Stockwell, B.R. (2000). Chemical genetics: ligand-based discovery of gene function. Nat. Rev. Genet. *1*, 116–125.
4. Wallace, B.A., and Janes, R.W. (2003). Circular dichroism and synchrotron radiation circular dichroism spectroscopy: tools for drug discovery. Biochem. Soc. Trans. *31*, 631–633.
5. Trewella, J. (1997). Insights into biomolecular function from small-angle scattering. Curr. Opin. Struct. Biol. *7*, 702–708.
6. Gruber, G. (2000). Structural and functional features of the Escherichia coli F1-ATPase. J. Bioenerg. Biomembr. *32*, 341–346.
7. Abele, R., Svergun, D., Keinanen, K., Koch, M.H., and Madden, D.R. (1999). A molecular envelope of the ligand-binding domain of a glutamate receptor in the presence and absence of agonist. Biochemistry *38*, 10949–10957.
8. Schonbrunn, E., Svergun, D.I., Amrhein, N., and Koch, M.H. (1998). Studies on the conformational changes in the bacterial cell wall biosynthetic enzyme UDP-N-acetylglucosamine enolpyruvyltransferase (MurA). Eur. J. Biochem. *253*, 406–412.
9. Hirai, M., Iwase, H., Hayakawa, T., Miura, K., and Inoue, K. (2002). Structural hierarchy of several proteins observed by wide-angle solution scattering. J. Synchrotron Radiat. *9*, 202–205.
10. Svergun, D., Barferato, C., and Koch, M.H.J. (1995). CRYSOL—a program to evaluate x-ray solution scattering of biological mac-

romolecules from atomic coordinates. J. Appl. Crystallogr. *28*, 768–773.
11. Holm, L., and Sander, C. (1998). Touring protein fold space with Dali/FSSP. Nucleic Acids Res. *26*, 316–319.
12. Jeffrey, P.D., Bewley, M.C., MacGillivray, R.T.A., Mason, A.B., Woodworth, R.C., and Baker, E.N. (1998). Ligand-induced conformational change in transferrins: crystal structure of the open form of the N-terminal half-molecule of human transferring. Biochemistry *37*, 13978–13986.
13. Baker, E.N., and Lindley, P.F. (1992). New perspectives on the structure and function of transferrins. J. Inorg. Biochem. *47(3–4)*, 147–160.
14. Zhang, Y., and Pardridge, W.M. (2001). Rapid transferring efflux from brain to blood across the blood-brain barrier. J. Neurochem. *76*, 1597–1600.
15. Sharff, A.J., Rodseth, L.E., Spurlino, J.C., and Quiocho, F.A. (1992). Crystallographic evidence of a large ligand-induced hinge-twist motion between the two domains of the maltodextrin binding protein involved in active transport and chemotaxis. Biochemistry *31*, 10657–10663.
16. Shilton, B.H., Flocco, M.M., Nilsson, M., and Mowbray, S.L. (1996). Conformational changes of three periplasmic receptors for bacterial chemotaxis and transport: the maltose-, glucose/galactose- and ribose-binding proteins. J. Mol. Biol. *264*, 350–363.
17. Gerstein, M., Lesk, A., and Chothia, C. (1994). Structural mechanisms for domain movements in proteins. Biochemistry *33*, 6739–6749.
18. Nelson, M.R., and Chazin, W.J. (1998). Calmodulin as a calcium sensor. In Calmodulin and Signal Transduction, L.J. Van Eldik and D.M. Watterson, eds. (Academic Press: San Diego), pp.17–64.
19. Jaren, O.R., Harmon, S., Chen, A.F., and Shea, M.A. (2000). *Paramecium* calmodulin mutants defective in ion channel regulation can bind calcium-induced conformation switching. Biochemistry *39*, 6881–6890.
20. Jaren, O.R., Kranz, J.K., Sorensen, B.R., Wand, A.J., and Shea, M.A. (2002). Calcium-induced conformational switching of *Paramecium* calmodulin provides evidence for domain coupling. Biochemistry *41*, 14158–14166.
21. Waggoner, D.W., and Bernlohr, D.A. (1990). In situ labeling of the adipocyte lipid binding protein with 3- [^{125}I] iodo-4-azido-N-hexadecylsalicylamide. Evidence for a role of fatty acid binding proteins in lipid uptake. J. Biol. Chem. *265*, 11417–11420.
22. Xu, Z., Bernlohr, D.A., and Banaszak, L.J. (1992). Crystal structure of recombinant murine adipocyte lipid-binding protein. Biochemistry *31*, 3484–3492.
23. LaLonde, J.M., Levenson, M.A., Roe, J.J., Bernlohr, D.A., and Banaszak, L.J. (1994). Adipocyte lipid-binding protein complexed with arachidonic acid. Titration calorimetry and X-ray crystallographic studies. J. Biol. Chem. *269*, 25339–25347.
24. Olsnes, S., and Pihl, A. (1972). Ricin—a potent inhibitor of protein synthesis. FEBS Lett. *20*, 327–329.
25. Endo, Y., and Tsurugi, K. (1987). RNA N-glycosidase activity of ricin A-chain. Mechanism of action of the toxic lectin ricin on eukaryotic ribosomes. J. Biol. Chem. *262*, 8128–8130.
26. Rutenber, E., and Robertus, J.D. (1991). Structure of ricin B-chain at 2.5 Å resolution. Proteins *10*, 260–269.
27. Weston, S.A., Tucker, A.D., Thatcher, D.R., Derbyshire, D.J., and Pauptit, R.A. (1994). X-ray structure of recombinant ricin A-chain at 1.8 Å resolution. J. Mol. Biol. *244*, 410–422.
28. Day, P.J., Ernst, S.R., Frankel, A.E., Monzingo, A.F., Pascal, J.M., Molina-Svinth, M.C., and Robertus, J.D. (1996). Structure and activity of an active site substitution of ricin A chain. Biochemistry *35*, 11098–11103.
29. Yan, X., Hollis, T., Svinth, M., Day, P., Monzingo, A.F., Milne, G.W., and Robertus, J.D. (1997). Structure-based identification of a ricin inhibitor. J. Mol. Biol. *266*, 1043–1049.
30. Skrynnikov, N.R., Goto, N.K., Yang, D., Choy, W.-Y., Tolman, J.R., Mueller, G.A., and Kay, L.E. (2000). Orienting domains in proteins using dipolar couplings measured by liquid-state NMR: differences in solution and crystal forms of maltodextrin binding protein loaded with β-cyclodextrin. J. Mol. Biol. *295*, 1265–1273.
31. Shilton, B.H., Flocco, M.M., Nilsson, M., and Mowbray, S.L. (1996). Conformational changes of three periplasmic receptors for bacterial chemotaxis and transport: the maltose-, glucose/galactose- and ribose-binding proteins. J. Mol. Biol. *264*, 350–363.
32. Irving, T.C., Fischetti, R.F., Rosenbaum, G., and Bunker, G.B. (2000). Fiber diffraction using the BioCAT undulator beamline at the advanced photon source. Nucleic Instr. Methods *448*, 250–254.
33. Hammersley, A.P., Svensson, S.O., Hanfland, M., Fitch, A.N., and Häusermann, D. (1996). Two-dimensional detector software: from real detector to idealised Iimage or two-theta scan. High Press. Res. *14*, 235–248.
34. Hammersley, A.P. (1997). ESRF Internal Report, ESRF97HA02T, "FIT2D: An Introduction and Overview."
35. Hammersley, A.P. (1998). ESRF Internal Report, ESRF98HA01T, FIT2D V9.129 Reference Manual V3.1.
36. DeLano, W.L. (2002). The PyMOL User's Manual (San Carlos, CA: DeLano Scientific).